JACS Au
AN OPEN ACCESS JOURNAL OF THE AMERICAN CHEMICAL SOCIETY

pubs.acs.org/jacsau

Article

Composition Dictates Molecular Orientation at the Heterointerfaces of Vapor-Deposited Glasses

Thomas J. Ferron, Marie E. Fiori, M. D. Ediger, Dean M. DeLongchamp,* and Daniel F. Sunday*

Cite This: *JACS Au* 2023, 3, 1931−1938

Read Online

ACCESS | Metrics & More | Article Recommendations | Supporting Information

ABSTRACT: Physical vapor deposition (PVD) can prepare organic glasses with a preferred molecular orientation. The relationships between deposition conditions and orientation have been extensively investigated in the film bulk. The role of interfaces on the structure is less well understood and remains a key knowledge gap, as the interfacial region can govern glass stability and optoelectronic properties. Robust experimental characterization has remained elusive due to complexities in interrogating molecular organization in amorphous, organic materials. Polarized soft X-rays are sensitive to both the composition and the orientation of transition dipole moments in the film, making them uniquely suited to probe molecular orientation in amorphous soft matter. Here, we utilize polarized resonant soft X-ray reflectivity (P-RSoXR) to simultaneously depth profile the composition and molecular orientation of a bilayer prepared through the physical vapor deposition of 1,4-di-[4-(*N*,*N*-diphenyl)amino]styryl-benzene (DSA-Ph) on a film of aluminum-tris(8-hydroxyquinoline) (Alq3). The bulk orientation of the DSA-Ph layer is controlled by varying deposition conditions. Utilizing P-RSoXR to depth profile the films enables determination of both the bulk orientation of DSA-Ph and the orientation near the Alq3 interface. At the Alq3 surface, DSA-Ph always lies with its long axis parallel to the interface, before transitioning into the bulk orientation. This is likely due to the lower mobility and higher glass transition of Alq3, as the first several monolayers of DSA-Ph deposited on Alq3 appear to behave as a blend. We further show how orientation at the interface correlates with the bulk behavior of a codeposited glass of similar blend composition, demonstrating a straightforward approach to predicting molecular orientation at heterointerfaces. This work provides key insights into how molecules orient during vapor deposition and offers methods to predict this property, a critical step toward controlling interfacial behavior in soft matter.

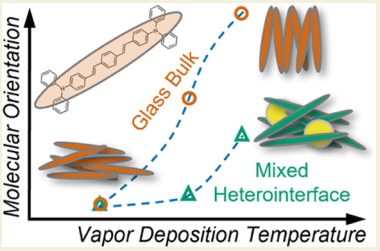

KEYWORDS: *glasses, vapor deposition, organic interfaces, reflectivity, soft X-rays, X-ray spectroscopy*

INTRODUCTION

Physical vapor deposition (PVD) of organic glasses has enabled the preparation of nonequilibrium thin films with birefringent optical properties.[1] Optical birefringence can be described with an index of refraction that depends on the polarization of the incident electric field vector and, in a PVD glass, is commonly observed when molecules adopt an anisotropic molecular packing.[2,3] PVD glasses with birefringence are prepared by directly depositing molecules onto the free surface where they have enhanced mobility compared to the bulk,[4] enabling them to achieve energetically favorable configurations prior to vitrification.[5] The subsequent layer-by-layer assembly thus results in a glass with bulk properties that mimic those favorable at the free surface. Exquisite control over the bulk molecular orientation can thus be achieved with PVD by manipulating this surface equilibration mechanism through processing conditions, such as varying the substrate temperature (T_{sub}) below the glass phase transition temperature (T_g) or changing the deposition rate.[6−8] In addition to birefringence, PVD glasses have been shown to demonstrate increased bulk density,[9,10] enhanced kinetic stability,[11,12] and advantageous optoelectronic and mechanical properties.[13−15]

Experimental characterization of this molecular orientation, and its influence on material properties, primarily comes from bulk thin-film measurements. However, understanding the interfacial structure is crucial to the development of novel functionality in soft matter. For example, the orientation of semiconducting organic molecules can influence the local density of states across an interface[16,17] as well as improve charge injection and interlayer transport in optoelectronic devices.[18,19] In addition, because glasses prepared through PVD can be more stable than ordinary glasses, the transformation into supercooled liquids proceeds via a front-mediated melting process that initiates at interfaces.[12,20] Methods to reinforce stability through inhibiting this growth front have been proposed, such as capping glass layers with high T_g materials, yet the front initiation process is not well understood at interfaces other than the free surface.[21]

Received: April 6, 2023
Revised: May 22, 2023
Accepted: June 9, 2023
Published: June 23, 2023

https://doi.org/10.1021/jacsau.3c00168
JACS Au 2023, 3, 1931−1938

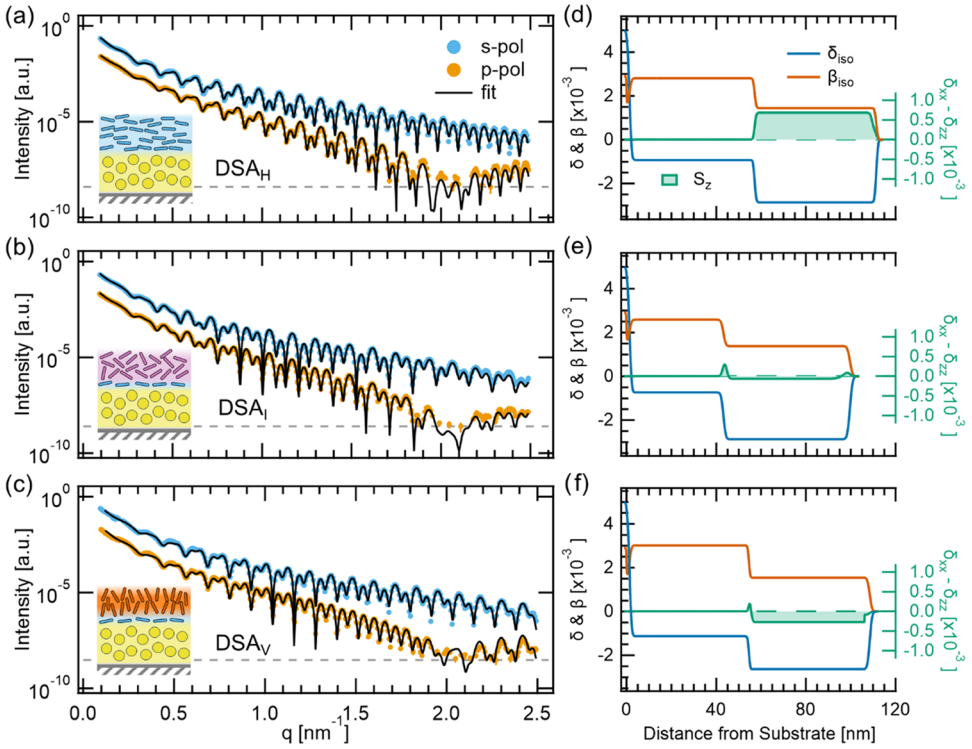

Figure 1. P-RSoXR of each bilayer glass measured in this study. (a−c) Data (circles) and model fits (black solid lines) for s- and p-polarization taken at 284.4 eV. P-polarization has been offset for clarity and is accompanied by a gray dashed line, indicating the lowest intensity measurable in this experiment. Data uncertainty is determined by Poisson counting statistics using the total number of counts measured on the CCD over a given exposure. Uncertainties are smaller than marker sizes shown. Inset cartoons present a qualitative schematic of the modeled structure as described in the text. Rods represent DSA-Ph (oriented according to the long axis), and circles represent Alq3. (d−f) Complex index of refraction (left axis, real—blue and imaginary—orange) and birefringence (right axis, green) plotted as a function of film depth measured from the $SiliSiO_2$ interface.

Unfortunately, experimental techniques such as variable angle spectroscopic ellipsometry (VASE) have too low a spatial resolution for the sharp (∼1 nm) interfaces generated by PVD, and diffractive techniques have been unable to identify the molecular packing that may occur within a mixed interface.[22] Our capability to fundamentally understand potential emergent behaviors rely on detailed characterization of both composition and molecular orientation distributions across interfaces.

In this study, we use polarized resonant soft X-ray reflectivity (P-RSoXR) to characterize the molecular orientation expressed at heterointerfaces in PVD glass. P-RSoXR is an emerging reflectometry technique that leverages soft X-rays to greatly enhance molecular contrast by probing near-edge X-ray absorption fine structure (NEXAFS) transition dipoles.[23−29] This sensitivity to NEXAFS transitions enables P-RSoXR to depth profile chemical composition and molecular orientation in thin films with nanoscale sensitivity.[30] Presently, soft matter investigations that utilize P-RSoXR have thus far been limited to studying either multicomponent heterostructures comprised of isotropically oriented materials[24,25,31] or chemically homogeneous films with orientation heterogeneities.[23,29] Herein, for the first time, P-RSoXR is used to construct simultaneous composition and molecular orientation depth profiles in layered structures of amorphous organic materials. This critical advancement enables P-RSoXR to provide unique insights into the complementary roles of molecular orientation and composition in developing structure−function relationships within thin-film multilayer devices. Measurements are conducted on PVD glass bilayers of aluminum-tris(8-hydroxyquinoline) (Alq3) and 1,4-di-[4-(*N*,*N*-diphenyl)-amino]styryl-benzene (DSA-Ph) to characterize a 1−2 nm interfacial width, with the goal of understanding how anisotropic molecules orient at buried heterointerfaces. From our measurements, we determine that the interfacial structure of a PVD bilayer matches the bulk properties of a blended glass as if the two components had been codeposited and our results suggest opportunities to predict such interfacial characteristics that govern advanced device functionality.

EXPERIMENTAL METHODS

Sublimed grade Alq3 (99.995% trace metals basis) was purchased from Sigma-Aldrich, and DSA-Ph (>99%) was purchased from Luminescence Technology Corp. Both materials were used as received. Silicon substrates, ⟨100⟩ with 1−2 nm native oxide, were precleaned prior to sample preparation by sonicating in subsequent baths of acetone and isopropyl alcohol followed by exposure to UV-Ozone. PVD was carried out in a custom vacuum deposition system with a nominal base pressure of ≈10^{-4} Pa with details described in past publications.[32] The deposition rate was maintained at 0.2 nm/s and monitored with a quartz crystal microbalance. Fabricated thin films contain a small thickness gradient due to the deposition geometry resulting in an ≈2 nm change in thickness over a 1 cm distance.[29] Molecular orientation was manipulated by varying T_{sub} as described in the main text.

P-RSoXR was conducted at beamline 11.0.1.2 at the Advanced Light Source.[33] Measurements were carried out at fixed photon energy and polarization, either perpendicular (s-polarization) or parallel (p-polarization) to the plane of incidence, while varying the angle of incidence, θ, from 1 to 60° in a θ−2θ configuration. The specular reflectance was collected on a CCD and corrected for background counts and exposure before normalizing with the direct beam intensity. A small beam spot (≈100 μm full width at half-

https://doi.org/10.1021/jacsau.3c00168
JACS Au 2023, 3, 1931−1938

maximum (FWHM)) was used alongside a large sample size (≈30 mm) to forgo the need for a footprint correction and limit the sample thickness variation to several angstroms. Fitting P-RSoXR was carried out using a custom modeling package compatible with the analysis tool *refnx*, and a Differential Evolution Markov Chain Monte Carlo sampler was used for model optimization.[34,35] Polarized reflectivity was fit as a function of the momentum transfer vector ($q = 4\pi/\lambda \sin(\theta)$, where λ is the wavelength) according to an anisotropic transfer matrix formalism.[36] Both polarizations are fitted simultaneously to the same slab model to extract molecular composition and orientation-induced birefringence as a function of film depth. All parameter uncertainties are defined by the 95% confidence interval of the fitted posterior distributions.

RESULTS AND DISCUSSION

We investigated a series of model PVD bilayers comprising two glassy organic semiconductors in order to study molecular organization at device-relevant interfaces. Subsequent layers of Alq3 (T_g = 450 K), an electron-transport molecule,[37] and DSA-Ph (T_g = 360 K), a blue organic light-emitting diode (OLED) emitter,[38] were prepared by PVD on silicon substrates for P-RSoXR measurements. T_{sub} was varied to manipulate the bulk orientation of DSA-Ph in each of the three glasses studied following previously prescribed methods that have identified a T_{sub}/T_g ratio of 0.9 where the bulk orientation will transition from nominally horizontal to vertical.[6,22] Alq3 and DSA-Ph depositions were carried out at T_{sub} = 290 K, T_{sub} = 330 K, and T_{sub} = 343 K to assemble horizontal (parallel, T_{sub}/T_g = 0.80), isotropic (T_{sub}/T_g = 0.92), and vertical (perpendicular, T_{sub}/T_g = 0.95) orientations of the DSA-Ph long axis with respect to the plane of the substrate. Samples throughout this study will be labeled DSA_i where i designates the previously established bulk orientation for these substrate temperatures: horizontal (H), isotropic (I), or vertical (V).

In Figure 1, we summarize the P-RSoXR results of each sample measured at 284.4 eV with two orthogonal X-ray polarizations. This energy was selected to optimize DSA-Ph birefringence (using experimental NEXAFS spectra as a guide, see arrows in Figure 3) while minimizing the onset of absorption from the C=C 1s → π* resonance near 285.1 eV. Each profile exhibits Kiessig fringes that, due to resonance, not only result from reflections at heterointerfaces (Si|SiO_2, SiO_2|Alq3, Alq3|DSA-Ph, and DSA-Ph|Vacuum) but also become convoluted by interfaces between different DSA-Ph orientations. To fit the P-RSoXR data, our models consist of a Si substrate with a SiO_2 native surface, a slab of Alq3, and up to three slabs composed of DSA-Ph where we allow for the molecular orientation of each slab to vary. Optical properties are modeled with a uniaxial complex tensor index of refraction, $n(E) = 1 - \delta(E) + i\beta(E)$, defined with the ordinary axis (subscript xx) aligned in the plane of the substrate and extraordinary axis (subscript zz) perpendicular. A complimentary data set was collected at 285.8 eV to ensure our model is self-consistent between different energies and therefore different degrees of orientation contrast. Structural features are consistent between modeling efforts using both energies. Details on fitting methodologies and slab models can be found in the Supporting Information.

Based on fits to the data in Figure 1a−c, composition and molecular orientation depth profiles are constructed and given in Figure 1d−f. The composition of each layer is represented by scalars given by $\delta_{iso} = 1/3 \times (2\delta_{xx} + \delta_{zz})$ and $\beta_{iso} = 1/3 \times (2\beta_{xx} + \beta_{zz})$, which is equivalent to the index of refraction for a net isotropic organization (when $\delta_{xx} - \delta_{zz} = 0$ and $\beta_{xx} - \beta_{zz} = 0$, as defined in the Supporting Information). Both δ_{iso} and β_{iso} are open fitting parameters and all samples achieve a global minimum with comparable results. We can verify the molecular identity in each modeled slab by comparing extracted parameters with experimental NEXAFS given in the Supporting Information. Alq3 is easily verified in the bottom slab through its distinct π* resonance just below 284.5 eV, resulting in an enhanced β_{iso} and less negative δ_{iso} than DSA-Ph at 284.4 eV. Fits determine layer thicknesses of 55.83 ± 0.01, 41.89 ± 0.05, and 52.23 ± 0.03 nm for Alq3 and 54.26 ± 0.01, 57.3 ± 0.3, and 53.9 ± 0.2 nm for DSA_H, DSA_I, and DSA_V respectively, in agreement with VASE given in the Supporting Information. Free surface roughness for all samples was found to be nearly atomically smooth in agreement with past characterization on glassy DSA-Ph films and is reported in the Supporting Information.[22,32] P-RSoXR additionally reveals minimal intermixing at the interface between the two organic layers. Each Alq3|DSA-Ph interface is described according to Nevot & Croce with a roughness parameter, σ_r, and full interfacial width $w = \sqrt{2\pi}\sigma_r$[39] Each sample has a characteristically sharp interface given by 1.40 ± 0.01, 2.07 ± 0.01, and 1.15 ± 0.01 nm for DSA_H, DSA_I, and DSA_V, respectively. This interface represents the convolution of the vertical distribution in the chemical composition and the fluctuations in the interface position over the size of the beam spot. If we consider the approximate size of an individual molecule, our results indicate that the interface only encompasses 1−2 molecular layers. Neutron reflectivity experiments by Gentle and coworkers have offered a similar description of the interface involving vapor-deposited (deuterated) Alq3 and a low T_g glassy blend with $\sigma_r \approx 0.5$ nm ($w \approx 1.3$ nm).[40]

In P-RSoXR, the molecular orientation is related to the fitted birefringence parameter, $(\delta_{xx} - \delta_{zz})$.[23,29] Alq3 was confirmed to be isotropic ($\delta_{xx} - \delta_{zz} = 0$) through P-RSoXR of a single layer deposited at T_{sub} = 290 K, and the Alq3 layer in the bilayer models were constrained based on this measurement. The index of refraction only becomes birefringent when the profiles transition from the Alq3 layer into the DSA-Ph layer with several key characteristics. The bulk of the DSA-Ph layer can be described as a uniform slab and an inverse relationship is found between the three samples, where increasing T_{sub} results in a more negative birefringence (a result that we will show correlates with the expected molecular orientation based on deposition conditions). The surface is found to be less birefringent than the bulk, a behavior that we have previously attributed to free-surface aging or adventitious hydrocarbon contamination.[29] Intriguingly, optimized models find a positive birefringence across all Alq3|DSA-Ph interfaces regardless of the glass preparation. We applied alternative models to DSA_I and DSA_V that enforce the bulk and interface to have the same birefringence and find that they are insufficient in describing the data, see the Supporting Information. This result suggests the interfacial molecular orientation is dissimilar to the bulk, but further quantitative analysis requires us to consider how the molecular geometry influences the alignment of resonant transition dipoles.[23,29]

Birefringence alone cannot be used to determine the internal molecular orientation. For this reason, we use NEXAFS spectroscopy to independently determine a three-dimensional (3D) tensor index of refraction and translate the birefringence measured from P-RSoXR into a molecular orientation. We will briefly describe our methodology and the major assumptions used in our analysis here, and more details can be found in the

https://doi.org/10.1021/jacsau.3c00168
JACS Au 2023, 3, 1931−1938

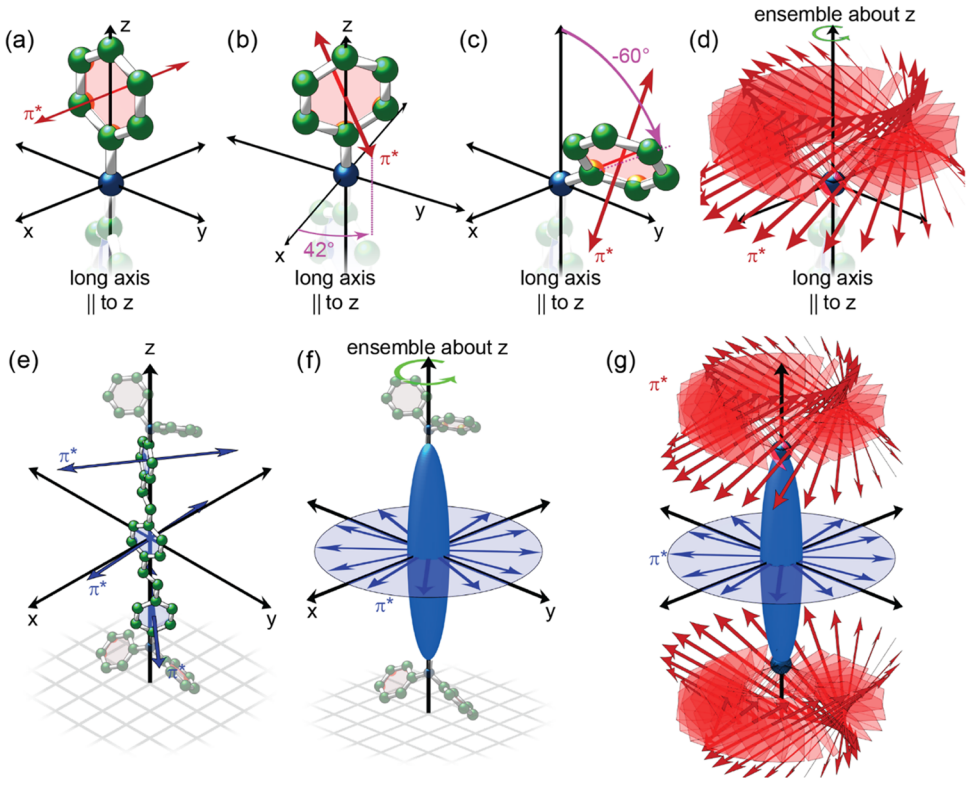

Figure 2. Schematic of conformational considerations to calculate a DSA-Ph tensor index of refraction. (a−c) Diphenylamine rotations to calculate the relative alignment of transition dipoles with respect to the long axis. (d) An ensemble of rotations about the molecular long axis accounts for amorphousness. (e, f) Planar dipole resulting from core phenyl groups. (g) Full geometry and symmetry considerations used in calculating the tensor index of refraction.

Supporting Information and in past publications.[23,29,41] Angle-dependent NEXAFS identifies a resonance at 285.1 eV with the highest observable absorption dichroism, see the Supporting Information, for which we assign the combined phenyl C═C 1s → π^* transition. The resonance with this moiety is key to determining molecular orientation as this dipole moment is perpendicular to the phenyl ring plane.[41,42] In Figure 2, we consider how the molecular conformation of a single DSA-Ph molecule will influence the tensor properties of this resonance. Previous quantum chemical calculations have determined that the distyrylarylene core is nearly coplanar and the diphenylamine end-groups exhibit a propeller-like conformation.[38] The core phenyl C═C 1s → π^* transition dipoles will thus extend perpendicular to the long axis of the molecule; however, the phenyl groups found in diphenylamine are tilted 60° off the molecular "long axis" (assuming a C−N−C bond angle of 120°) with a dihedral angle of ≈42°, see Figure 2a−c. This geometry guarantees that some contribution of the phenyl C═C 1s → π^* dipole moment will be parallel to the DSA-Ph long axis, reducing the expected dichroism from the full molecule.

P-RSoXR additionally measures a volume-average distribution of DSA-Ph orientations, and our tensor must account for the full population of probed molecules. From grazing incidence X-ray diffraction (GIXD), see the Supporting Information, it is evident that our samples do not exhibit any crystallinity that would restrict molecular packing, so we assume that any fixed rotation about the molecular long axis will be equally probable, see Figure 2e−g. Finally, any in-plane alignment will be isotropic, and the final tensor must be averaged about the substrate normal.[6,23,43] The full representative tensor index of refraction can be found in the Supporting Information.

In Figure 3, we present the birefringence from our calculated tensor as a function of the photon energy and molecular

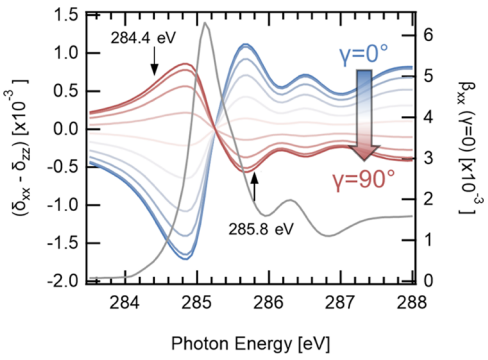

Figure 3. Representative γ-isoclines for the uniaxial tensor of DSA-Ph in increments of 10° (left axis). Black arrows indicate energies where P-RSoXR was measured. The right axis overlays β_{xx} (in gray) at γ = 0 for comparison.

orientation. We have defined the net molecular orientation as the angle between the substrate normal and the DSA-Ph long axis, γ. From this series of γ-isoclines, we find that at 284.4 eV, a positive DSA-Ph birefringence corresponds to a net horizontal alignment (γ > 54.7°), while a negative birefringence corresponds to a vertical alignment (γ < 54.7°). If we reexamine our orientation depth profiles using Figure 3 as a guide, T_{sub} < 0.9 T_g leads to DSA-Ph lying flat (horizontal), while 0.9 T_g < T_{sub} < 0.95 T_g results in DSA-

https://doi.org/10.1021/jacsau.3c00168
JACS Au 2023, 3, 1931−1938

Ph standing upright (vertical). As we alluded earlier, this result coincides with the past characterization of these molecules and the molecular tilts extracted are in excellent agreement with our own VASE measurements.[6,7,22] Having established that our tensor index of refraction can determine the molecular orientation of DSA-Ph from birefringence, we can further investigate the properties of the Alq3|DSA-Ph interface.

Figure 4a compares birefringence to the Alq3 volume fraction, φ_{Alq3} (where $\varphi_{DSA\text{-}Ph} = 1 - \varphi_{Alq3}$) for each sample as a

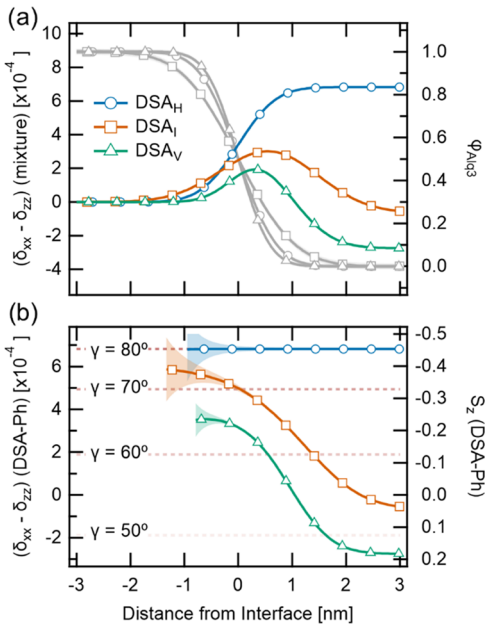

Figure 4. (a) Birefringence from best-fit models and the Alq3 volume fraction (gray) measured from P-RSoXR centered on the Alq3|DSA-Ph interface. Volume fraction profiles correspond to the marker shape in the figure legend. (b) Calculated birefringence (left axis) and S_z (right axis) due to DSA-Ph. The shaded region represents the calculated uncertainty propagated from best-fit models. Traces begin when DSA-Ph occupies 5% of the total volume. Dashed lines correspond to γ-isoclines given in Figure 3 at 284.4 eV for reference. Colored legend applies to parts (a, b).

function of distance from the Alq3|DSA-Ph interface. Because Alq3 is isotropic, the entirety of this birefringence results from oriented DSA-Ph. A two-phase model allows us to disentangle the contribution of each material relative to their respective volume fraction, such that $n_{mix}(E) = \sum_i \varphi_i n_i(E)$, where φ_i is the volume fraction and $n_i(E)$ is the dielectric tensor for the ith component. The resulting birefringence profile of DSA-Ph alone is given in Figure 4b. Our results indicate that in DSA$_I$ and DSA$_V$, the orientation transitions from a horizontal alignment near the interface, when DSA-Ph is mixed with Alq3, to the expected bulk orientation, either preferentially isotropic or vertical. In DSA$_H$, our best-fit model describes a constant orientation throughout the interface and bulk. We attribute this to pure DSA-Ph prepared at T_{sub} = 290 K already exhibiting a limiting horizontal orientation, and any mixing with Alq3 at this temperature cannot further increase the birefringence as seen in our other samples.[6,7]

This interfacial behavior is reminiscent of how glassy molecules lay flat when codeposited with high T_g materials. Work by Brütting and co-workers studied this phenomenon in OLED active layers where it is advantageous to align the optical dipole of emitter molecules in order to improve light outcoupling.[14,44] They found that when a small concentration of molecules is doped within a host matrix, the molecular orientation of the dopant becomes dependent on the T_g of the host.[45] Jiang et al. expanded upon this observation by studying mixed, two-component glasses of DSA-Ph codeposited with Alq3. They found that the full range of DSA-Ph orientations could be achieved by appropriately tuning the $T_{sub}/T_{g,mix}$ ratio, where $T_{g,mix}$ refers to the glass transition of the mixture, which is a function of the blend ratio.[46] As Alq3 has a greater T_g than DSA-Ph, a high concentration of Alq3 increases $T_{g,mix}$ and will prevent DSA-Ph from reorienting once adsorbed to the surface, resulting in a horizontal orientation.

To help compare our results to these previous studies, we convert our measured birefringence into the order parameter S_z, which is defined as follows

$$S_z = \frac{1}{2}(3\langle\cos^2\gamma\rangle - 1) \quad (1)$$

where $\langle\cdots\rangle$ indicates the average of the orientation distribution about γ. This parameter varies from $S_z = -0.5$ ($\gamma = 90$) for perfectly horizontal alignment to $S_z = 1$ ($\gamma = 0$) for perfectly vertical alignment ($S_z = 0$ is isotropic).[6] In Figure 5, we

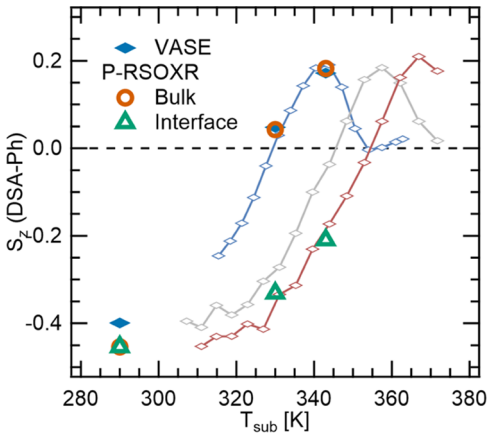

Figure 5. Orientation order parameter for all samples as a function of substrate temperature. VASE (solid blue diamonds) was determined from the DSA-Ph layers in this study. P-RSoXR is divided into the bulk (open orange circles) and interface (open green triangles), which is defined at φ_{Alq3} = 0.5 from Figure 4. Solid lines are taken from ref 46 and present the order parameter measured with infrared spectroscopy of DSA-Ph codeposited with Alq3 at 0% (open blue diamonds), 26% (open gray diamonds), and 42% (open red diamonds) blend concentrations.

compare our measured S_z to infrared spectroscopy (IR) from Jiang et al. and find excellent agreement between the bulk S_z values from all three experiments: P-RSoXR, VASE, and IR (from ref 46). Remarkably, the DSA-Ph orientation across the bilayer heterointerface (data from Figure 4b at φ_{Alq3} = 0.5, labeled interface) shows excellent consistency with the bulk orientation found in codeposited glasses of similar blend compositions.

We can rationalize the consistency between our measured interfacial orientation and the codeposited glasses from Jiang et al. by comparing the preparation of the different glasses. According to the surface equilibration mechanism, there will remain a population of Alq3 at the free surface that remains mobile upon beginning the DSA-Ph deposition. We hypothesize that this coexistence of mobile DSA-Ph and Alq3 at the

https://doi.org/10.1021/jacsau.3c00168
JACS Au 2023, 3, 1931−1938

interface enables interdiffusion between the two species and the composition of this mobile layer is likely indistinguishable from a codeposited glass. However, unlike in codeposition, as the film transitions away from the Alq3 substrate, the remaining DSA-Ph will behave as a single-component glass as demonstrated in our orientation depth profiles. This mechanism would suggest that the bulk properties of a codeposited glass act as a representative structure of a similarly composed heterointerface. With the correlations outlined in Figure 5, one could predict the interfacial behavior of a multilayer glass with a thorough characterization of codeposited glasses prepared under similar conditions.

Our proposed mechanism is further supported by previous investigations. Fiori et al. studied molecular packing in superlattices of alternating DSA-Ph and Alq3 layers. They found that beyond a 1−2 nm interface, DSA-Ph was not influenced by the underlying Alq3, in excellent agreement with our P-RSoXR depth profiles.[22] Simulations by Yoo et al. studied bilayers composed of the linear molecules CBP, α-NPD, or BSB-Cz under conditions that resulted in a preferred net horizontal alignment for all molecules.[47] Only a small deviation from the bulk orientation was observed at each interface, but molecules that fully diffused into the adjacent layer were found to orient similarly to the host. In all cases, the extent of horizontal orientation (magnitude of S_z) at the interface would increase (decrease) when the opposing molecule had a higher (lower) T_g. This result qualitatively agrees with our hypothesis, the T_g of the interfacial layer is averaged over the local composition during preparation, and the orientation would follow from the $T_{sub}/T_{g,mix}$ ratio, as observed by Jiang et al. Molecular dynamics simulations that explore molecules with a larger differential T_g or differently shaped molecules would provide valuable insights to better understand this interfacial property in PVD glass.

The results discussed here assume that the molecular geometry of DSA-Ph follows the characteristics of an isolated molecule. However, it is unlikely that this conformation will remain unaffected upon condensing into a solid. Other π-conjugated molecules that contain triphenylamine as a building block have shown an increase in planarity upon adsorbing onto gold substrates.[48,49] In fact, we note that for DSA_H, S_z measured with P-RSoXR is greater than that measured from VASE (and with a lesser magnitude, DSA_I and DSA_V). If instead, we were to consider an optical model where the dihedral angle in diphenylamine was ≈30°, we recover quantitative consistency between the two measurements as achieved in past studies.[23,29] Another important consideration is that we are likely investigating the distribution of conformations, and P-RSoXR is only sensitive to the mean dipole moment. We can again recover quantitative consistency between P-RSoXR and VASE by considering a population where ≈30% of molecules have all phenyl rings coplanar and in ≈70%, diphenylamine exhibits an isotropic dihedral distribution. We want to stress here that this ambiguity does not influence the structural characteristics of our slab model, and results derived from the relative magnitude and sign of the birefringence (orientation) are unaffected by these considerations.

CONCLUSIONS

In conclusion, we investigated the depth dependence of composition and molecular orientation simultaneously in a series of vapor-deposited organic glasses using P-RSoXR. In all conditions studied, DSA-Ph was found to predominately orient horizontally while intermixing with Alq3 at a heterointerface. Furthermore, the bulk orientation was not influenced by any underlying structure in agreement with past studies. Our results suggest that the mobile surface layer, as described by the surface equilibrium mechanism, is nearly indistinguishable between a codeposited glass and at a heterointerface, leading to a similar structure between the two. We believe that this study will promote further investigations into the interfacial behavior of PVD glasses to help develop critical structure−function relationships and study the fundamental behavior of glasses that occurs at buried interfaces.

ASSOCIATED CONTENT

Supporting Information

The Supporting Information is available free of charge at https://pubs.acs.org/doi/10.1021/jacsau.3c00168.

Results from variable angle spectroscopic ellipsometry; angle-dependent near-edge X-ray absorption fine structure (NEXAFS) spectroscopy; grazing incidence X-ray diffraction; and complementary polarized resonant soft X-ray reflectivity modeling as well as the methodology for calculating the NEXAFS-derived complex tensor index of refraction (PDF)

AUTHOR INFORMATION

Corresponding Authors

Dean M. DeLongchamp − *National Institute of Standards and Technology, Gaithersburg, Maryland 20899, United States;* orcid.org/0000-0003-0840-0757; Email: deand@nist.gov

Daniel F. Sunday − *National Institute of Standards and Technology, Gaithersburg, Maryland 20899, United States;* orcid.org/0000-0002-6840-535X; Email: daniel.sunday@nist.gov

Authors

Thomas J. Ferron − *National Institute of Standards and Technology, Gaithersburg, Maryland 20899, United States;* Present Address: Lawrence Livermore National Laboratory, Livermore, California 94550, United States; orcid.org/0000-0002-2242-2648

Marie E. Fiori − *Department of Chemistry, University of Wisconsin−Madison, Madison, Wisconsin 53706, United States;* orcid.org/0000-0002-8020-063X

M. D. Ediger − *Department of Chemistry, University of Wisconsin−Madison, Madison, Wisconsin 53706, United States;* orcid.org/0000-0003-4715-8473

Complete contact information is available at: https://pubs.acs.org/10.1021/jacsau.3c00168

Funding

T.J.F. was supported by the National Research Council fellowship, and parts of this manuscript were finalized under the auspices of the U.S. Department of Energy (DOE) at Lawrence Livermore National Laboratory under Contract No. DE-AC52-07NA27344. The University of Wisconsin-Madison was supported by the U.S. Department of Energy, Office of Basic Energy Science, Division of Materials Science and Engineering Award DESC0002161. The use of beamline 11.0.1.2 at the Advanced Light Source was supported by the

U.S. Department of Energy (DOE) Office of Science User Facility under contract no. DEAC02−05CH11231. Part of this research was undertaken on the Soft X-ray spectroscopy beamline at the Australian Synchrotron, part of ANSTO. This research used beamline SST-1 and the Complex Materials Scattering of the National Synchrotron Light Source II, a U.S. Department of Energy (DOE) Office of Science User Facility operated for the DOE Office of Science by Brookhaven National Laboratory under Contract No. DE-SC0012704.

Notes

The authors declare no competing financial interest.

■ ACKNOWLEDGMENTS

The authors gratefully acknowledge the support of Cheng Wang for enabling remote access at the ALS for P-RSoXR measurements, as well as Jacob Thelen, Lars Tomson, and Eliot Gann for assistance in conducting NEXAFS measurements. The authors would also like to thank Lucas Flagg and Ruipeng Li for their assistance in setting up GIXD measurements. Certain commercial equipment, instruments, or materials (or suppliers, software, etc.) are identified in this paper to foster understanding. Such identification does not imply recommendation or endorsement by the National Institute of Standards and Technology nor does it imply that the materials or equipment identified are necessarily the best available for the purpose.

■ REFERENCES

(1) Ediger, M. D.; de Pablo, J.; Yu, L. Anisotropic Vapor-Deposited Glasses: Hybrid Organic Solids. *Acc. Chem. Res.* **2019**, *52*, 407−414.
(2) Yokoyama, D. Molecular orientation in small-molecule organic light-emitting diodes. *J. Mater. Chem.* **2011**, *21*, 19187−19202.
(3) Lyubimov, I.; Antony, L.; Walters, D. M.; Rodney, D.; Ediger, M. D.; de Pablo, J. J. Orientational anisotropy in simulated vapor-deposited molecular glasses. *J. Chem. Phys.* **2015**, *143*, No. 094502.
(4) Zhu, L.; Brian, C. W.; Swallen, S. F.; Straus, P. T.; Ediger, M. D.; Yu, L. Surface self-diffusion of an organic glass. *Phys. Rev. Lett.* **2011**, *106*, No. 256103.
(5) Liu, T.; Exarhos, A. L.; Alguire, E. C.; Gao, F.; Salami-Ranjbaran, E.; Cheng, K.; Jia, T.; Subotnik, J. E.; Walsh, P. J.; Kikkawa, J. M.; Fakhraai, Z. Birefringent Stable Glass with Predominantly Isotropic Molecular Orientation. *Phys. Rev. Lett.* **2017**, *119*, No. 095502.
(6) Dalal, S. S.; Walters, D. M.; Lyubimov, I.; de Pablo, J. J.; Ediger, M. D. Tunable molecular orientation and elevated thermal stability of vapor-deposited organic semiconductors. *Proc. Natl. Acad. Sci. U.S.A.* **2015**, *112*, 4227−4232.
(7) Bagchi, K.; Gujral, A.; Toney, M. F.; Ediger, M. D. Generic packing motifs in vapor-deposited glasses of organic semiconductors. *Soft Matter* **2019**, *15*, 7590−7595.
(8) Bishop, C.; Gujral, A.; Toney, M. F.; Yu, L.; Ediger, M. D. Vapor-Deposited Glass Structure Determined by Deposition Rate-Substrate Temperature Superposition Principle. *J. Phys. Chem. Lett.* **2019**, *10*, 3536−3542.
(9) Jin, Y.; Zhang, A.; Wolf, S. E.; Govind, S.; Moore, A. R.; Zhernenkov, M.; Freychet, G.; Shamsabadi, A. A.; Fakhraai, Z. Glasses denser than the supercooled liquid. *Proc. Natl. Acad. Sci. U.S.A.* **2021**, *118*, No. e2100738118.
(10) Ishii, K.; Nakayama, H.; Hirabayashi, S.; Moriyama, R. Anomalously high-density glass of ethylbenzene prepared by vapor deposition at temperatures close to the glass-transition temperature. *Chem. Phys. Lett.* **2008**, *459*, 109−112.
(11) Swallen, S. F.; Kearns, K. L.; Mapes, M. K.; Kim, Y. S.; McMahon, R. J.; Ediger, M. D.; Wu, T.; Yu, L.; Satija, S. Organic Glasses with Exceptional Thermodynamic and Kinetic Stabiliy. *Science* **2007**, *315*, 353−356.
(12) Flenner, E.; Berthier, L.; Charbonneau, P.; Fullerton, C. J. Front-Mediated Melting of Isotropic Ultrastable Glasses. *Phys. Rev. Lett.* **2019**, *123*, No. 175501.
(13) Ràfols-Ribé, J.; Willard, A. P.; Hänisch, C.; Gonzalez-Silverira, M.; Lenk, S.; Rodríguez-Viejo, J.; Reineke, S. High-performance organic light-emitting diodes comprising ultrastable glass layers. *Sci. Adv.* **2018**, *4*, No. eaar8332.
(14) Bagchi, K.; Ediger, M. D. Controlling Structure and Properties of Vapor-Deposited Glasses of Organic Semiconductors: Recent Advances and Challenges. *J. Phys. Chem. Lett.* **2020**, *11*, 6935−6945.
(15) Cang, Y.; Wang, Z.; Bishop, C.; Yu, L.; Ediger, M. D.; Fytas, G. Extreme Elasticity Anisotropy in Molecular Glasses. *Adv. Funct. Mater.* **2020**, *30*, No. 2001481.
(16) Duhm, S.; Heimel, G.; Salzmann, I.; Glowatzki, H.; Johnson, R. L.; Vollmer, A.; Rabe, J. P.; Koch, N. Orientation-dependent ionization energies and interface dipoles in ordered molecular assemblies. *Nat. Mater.* **2008**, *7*, 326−332.
(17) Chen, W.; Qi, D.-C.; Huang, H.; Gao, X.; Wee, A. T. S. Organic-Organic Heterojunction Interfaces: Effect of Molecular Orientation. *Adv. Funct. Mater.* **2011**, *21*, 410−424.
(18) Jailaubekov, A. E.; Willard, A. P.; Tritsch, J. R.; Chan, W. L.; Sai, N.; Gearba, R.; Kaake, L. G.; Williams, K. J.; Leung, K.; Rossky, P. J.; Zhu, X.-Y. Hot charge-transfer excitons set the time limit for charge separation at donor/acceptor interfaces in organic photovoltaics. *Nat. Mater.* **2013**, *12*, 66−73.
(19) Ndjawa, G. O. N.; Graham, K. R.; Li, R.; Conron, S. M.; Erwin, P.; Chou, K. W.; Burkhard, G. F.; Zhao, K.; Hoke, E. T.; Thompson, M. E.; et al. Impact of Molecular Orientation and Spontaneous Interfacial Mixing on the Performance of Organic Solar Cells. *Chem. Mater.* **2015**, *27*, 5597−5604.
(20) Swallen, S. F.; Traynor, K.; McMahon, R. J.; Ediger, M. D.; Mates, T. E. Stable glass transformation to supercooled liquid via surface-initiated growth front. *Phys. Rev. Lett.* **2009**, *102*, No. 065503.
(21) Sepúlveda, A.; Swallen, S. F.; Ediger, M. D. Manipulating the properties of stable organic glasses using kinetic facilitation. *J. Chem. Phys.* **2013**, *138*, No. 12A517.
(22) Fiori, M. E.; Bagchi, K.; Toney, M. F.; Ediger, M. D. Surface equilibration mechanism controls the molecular packing of glassy molecular semiconductors at organic interfaces. *Proc. Natl. Acad. Sci. U.S.A.* **2021**, *118*, No. e2111988118.
(23) Thelen, J. L.; Bishop, C.; Bagchi, K.; Sunday, D. F.; Gann, E.; Mukherjee, S.; Richter, L. J.; Kline, R. J.; Ediger, M. D.; DeLongchamp, D. M. Molecular Orientation Depth Profiles in Organic Glasses Using Polarized Resonant Soft X-ray Reflectivity. *Chem. Mater.* **2020**, *32*, 6295−6309.
(24) Loo, W. S.; Feng, H.; Ferron, T. J.; Ruiz, R.; Sunday, D. F.; Nealey, P. F. Determining Structure and Thermodynamics of A-b-(B-r-C) Copolymers. *ACS Macro Lett.* **2023**, *12*, 118−124.
(25) Sunday, D. F.; Chen, X.; Albrecht, T. R.; Nowak, D.; Rincon Delgadillo, P.; Dazai, T.; Miyagi, K.; Maehashi, T.; Yamazaki, A.; Nealey, P. F.; Kline, R. J. Influence of Additives on the Interfacial Width and Line Edge Roughness in Block Copolymer Lithography. *Chem. Mater.* **2020**, *32*, 2399−2407.
(26) Mezger, M.; Jérôme, B.; Kortright, J. B.; Valvidares, M.; Gullikson, E. M.; Giglia, A.; Mahne, N.; Nannarone, S. Molecular orientation in soft matter thin films studied by resonant soft x-ray reflectivity. *Phys. Rev. B* **2011**, *83*, No. 155406.
(27) Pasquali, L.; Mukherjee, S.; Terzi, F.; Giglia, A.; Mahne, N.; Koshmak, K.; Esaulov, V.; Toccafondi, C.; Canepa, M.; Nannarone, S. Structural and electronic properties of anisotropic ultrathin organic films from dichroic resonant soft x-ray reflectivity. *Phys. Rev. B* **2014**, *89*, No. 045401.
(28) Sunday, D. F.; Chan, E. P.; Orski, S. V.; Nieuwendaal, R. C.; Stafford, C. M. Functional group quantification of polymer nanomembranes with soft x-rays. *Phys. Rev. Mater.* **2018**, *2*, No. 032601.
(29) Ferron, T. J.; Thelen, J. L.; Bagchi, K.; Deng, C.; Gann, E.; de Pablo, J. J.; Ediger, M. D.; Sunday, D. F.; DeLongchamp, D. M. Characterization of the Interfacial Orientation and Molecular

https://doi.org/10.1021/jacsau.3c00168
JACS Au 2023, 3, 1931−1938

Conformation in a Glass-Forming Organic Semiconductor. *ACS Appl. Mater. Interfaces* **2022**, *14*, 3455−3466.
(30) Collins, B. A.; Gann, E. Resonant soft X-ray scattering in polymer science. *J. Polym. Sci.* **2022**, *60*, 1199−1243.
(31) Sunday, D. F.; Chang, A. B.; Liman, C. D.; Gann, E.; Delongchamp, D. M.; Thomsen, L.; Matsen, M. W.; Grubbs, R. H.; Soles, C. L. Self-Assembly of ABC Bottlebrush Triblock Terpolymers with Evidence for Looped Backbone Conformations. *Macromolecules* **2018**, *51*, 7178−7185.
(32) Bagchi, K.; Deng, C.; Bishop, C.; Li, Y.; Jackson, N. E.; Yu, L.; Toney, M. F.; de Pablo, J. J.; Ediger, M. D. Over What Length Scale Does an Inorganic Substrate Perturb the Structure of a Glassy Organic Semiconductor? *ACS Appl. Mater. Interfaces* **2020**, *12*, 26717−26726.
(33) Gann, E.; Young, A. T.; Collins, B. A.; Yan, H.; Nasiatka, J.; Padmore, H. A.; Ade, H.; Hexemer, A.; Wang, C. Soft x-ray scattering facility at the Advanced Light Source with real-time data processing and analysis. *Rev. Sci. Instrum.* **2012**, *83*, No. 045110.
(34) Ferron, T.; Sunday, D. F.. *pyPXR*, https://github.com/usnistgov/P-RSoXR, 2022. (accessed April 2022).
(35) Nelson, A. R. J.; Prescott, S. W. refnx: neutron and X-ray reflectometry analysis in Python. *J. Appl. Crystallogr.* **2019**, *52*, 193−200.
(36) Ignatovich, F. V.; Ignatovich, V. K. Optics of anisotropic media. *Phys.-Usp.* **2012**, *55*, 709−720.
(37) Halls, M. D.; Schlegel, H. B. Molecular Orbital Study of the First Excited State of the OLED Material Tris(8-hydroxyquinoline)-aluminum(III). *Chem. Mater.* **2001**, *13*, 2632−2640.
(38) Ho, M.-H.; Chang, C.-M.; Chu, T.-Y.; Chen, T.-M.; Chen, C. H. Iminodibenzyl-substituted distyrylarylenes as dopants for blue and white organic light-emitting devices. *Org. Electron.* **2008**, *9*, 101−110.
(39) Névot, L.; Croce, P. Caractérisation des surfaces par réflexion rasante de rayons X. Application à l'étude du polissage de quelques verres silicates. *Rev. Phys. Appl.* **1980**, *15*, 761−779.
(40) McEwan, J. A.; Clulow, A. J.; Nelson, A.; Yepuri, N. R.; Burn, P. L.; Gentle, I. R. Dependence of Organic Interlayer Diffusion on Glass-Transition Temperature in OLEDs. *ACS Appl. Mater. Interfaces* **2017**, *9*, 14153−14161.
(41) Mukherjee, S.; Streit, J. K.; Gann, E.; Saurabh, K.; Sunday, D. F.; Krishnamurthy, A.; Ganapathysubramanian, B.; Richter, L. J.; Vaia, R. A.; DeLongchamp, D. M. Polarized X-ray scattering measures molecular orientation in polymer-grafted nanoparticles. *Nat. Commun.* **2021**, *12*, No. 4896.
(42) Stohr, J. *NEXAFS Spectroscopy*; Springer, 1992.
(43) Gujral, A.; O'Hara, K. A.; Toney, M. F.; Chabinyc, M. L.; Ediger, M. D. Structural Characterization of Vapor-Deposited Glasses of an Organic Hole Transport Material with X-ray Scattering. *Chem. Mater.* **2015**, *27*, 3341−3348.
(44) Jurow, M. J.; Mayr, C.; Schmidt, T. D.; Lampe, T.; Djurovich, P. I.; Brutting, W.; Thompson, M. E. Understanding and predicting the orientation of heteroleptic phosphors in organic light-emitting materials. *Nat. Mater.* **2016**, *15*, 85−91.
(45) Naqvi, B. A.; Schmid, M.; Crovini, E.; Sahay, P.; Naujoks, T.; Rodella, F.; Zhang, Z.; Strohriegl, P.; Brase, S.; Zysman-Colman, E.; Brütting, W. What Controls the Orientation of TADF Emitters? *Front. Chem.* **2020**, *8*, No. 750.
(46) Jiang, J.; Walters, D. M.; Zhou, D.; Ediger, M. D. Substrate temperature controls molecular orientation in two-component vapor-deposited glasses. *Soft Matter* **2016**, *12*, 3265−3270.
(47) Yoo, D.; Song, H.; Youn, Y.; Jeon, S. H.; Cho, Y.; Han, S. A molecular dynamics study on the interface morphology of vapor-deposited amorphous organic thin films. *Phys. Chem. Chem. Phys.* **2019**, *21*, 1484−1490.
(48) Zhang, T.; Grazioli, C.; Guarnaccio, A.; Brumboiu, I. E.; Lanzilotto, V.; Johansson, F. O. L.; Beranová, K.; Coreno, M.; de Simone, M.; Brena, B.; et al. m-MTDATA on Au(111): Spectroscopic Evidence of Molecule−Substrate Interactions. *J. Phys. Chem. C* **2022**, *126*, 3202−3210.
(49) Zhang, T.; Svensson, P. H. W.; Brumboiu, I. E.; Lanzilotto, V.; Grazioli, C.; Guarnaccio, A.; Johansson, F. O. L.; Beranova, K.; Coreno, M.; de Simone, M.; et al. Clarifying the Adsorption of Triphenylamine on Au(111): Filling the HOMO-LUMO Gap. *J. Phys. Chem. C* **2022**, *126*, 1635−1643.

https://doi.org/10.1021/jacsau.3c00168
JACS Au 2023, 3, 1931−1938